Chemical Science

EDGE ARTICLE

View Article Online
View Journal | View Issue

Cite this: *Chem. Sci.*, 2019, **10**, 3346

All publication charges for this article have been paid for by the Royal Society of Chemistry

Photo-responsive cyclodextrin/anthracene/Eu^{3+} supramolecular assembly for a tunable photochromic multicolor cell label and fluorescent ink†

Weilei Zhou,[a] Yong Chen,[a] Qilin Yu,[ac] Peiyu Li,[a] Xuman Chen[a] and Yu Liu *[ab]

Received 3rd January 2019
Accepted 4th February 2019

DOI: 10.1039/c9sc00026g

rsc.li/chemical-science

A photo-responsive supramolecular assembly was successfully constructed through the stoichiometric 2 : 1 non-covalent association of two 4-(anthracen-2-yl)pyridine-2,6-dicarboxylic acid (**1**) units in one γ-cyclodextrin (γ-CD) cavity, followed by the subsequent coordination polymerization of the γ-CD·$\mathbf{1}_2$ ($\mathbf{1}_2$ = two **1**) inclusion complex with Eu(III). Interestingly, owing to the photodimerization behavior of anthracene units and the excellent luminescence properties of Eu(III), the $Eu^{3+}\subset$γ-CD·$\mathbf{1}_2$ system showed multicolor fluorescence emission from cyan to red by irradiation for 0–16 minutes. Moreover, white light emission with CIE coordinates (0.32 and 0.36) was achieved at 4 min. Importantly, white light-containing multicolor emission could be obtained in water, solid films and living cells. Especially, the $Eu^{3+}\subset$γ-CD·$\mathbf{1}_2$ system could tag living cells with marvelous white fluorescence and display no obvious cytotoxicity. Thus, this supramolecular assembly offers a new pathway in the fields of tunable photochromic fluorescent ink and cell labelling.

Introduction

Pseudorotaxanes and rotaxanes as typical species of molecular machines are challenging and interesting due to their mechanically interlocked topologies[1] and unique photophysical properties, leading to their wide application in biomedicine,[2] nanotechnology,[3] smart materials[4] and so on. In particular, functional fluorescent rotaxanes[5] are of major importance, which draw more and more attention from scientists and engineers. Multicolor emissions, especially white-light emission, have various applications in solid-state lighting[6] and display media owing to their superior color fidelity and low color distortion.[7] Generally, white light emission could be achieved by different methods in inorganic and organic materials.[7b,8] Among them, the mixing of several fluorophores with complementary emission colors becomes a popular strategy,[9] and the dynamic reversible properties of supramolecular systems and molecular assembly strategies play an important role. For instance, Tian *et al.*[10] reported a white-light emitting supramolecular assembly by changing the excitation wavelength and host–guest interactions in water. Tao *et al.*[11] reported a white-light emitting supramolecular polymer based on cucurbituril and oligo(*p*-phenylenevinylene) by altering different amounts of cucurbit[8]urils in the supramolecular assembly. Recently, we constructed host–guest complexes using dipolar dyes styrylpyridiniums and cucurbituril in which white-light emission was obtained by the addition of cucurbit[7]urils to methylated styrylpyridiniums for adjusting the stacking direction in water.[12]

Materials that respond to external photo-modulation, accompanied by changes in physicochemical properties have drawn much attention for extensive research because of their potential applications in various fields. Among all kinds of stimuli-responsive artificial devices, it is beneficial to design luminescent materials based on lanthanide ions due to their unique luminescence properties, such as long-lived excited states, visible-light emission and narrow emission bandwidths, which could be easy to distinguish from shorter-lived (ns-based) autofluorescence from biological materials.[13] Although multicolor luminescence has been reported several times recently, studies on *in situ* techniques are still rare,[7c] particularly photo-tuning single lanthanide ions for multicolor luminescence including white light in aqueous solution remains a challenge. Herein, combining a photo-tunable luminescent lanthanide,[13c] photo-erasable fluorescent ink[14] and cell imaging[15] of our previous reports, we designed a light-sensitive rotaxane network in aqueous solution from γ-cyclodextrin (γ-CD), 4-(anthracen-2-yl)pyridine-2,6-dicarboxylic acid (**1**) and Eu(III) as shown in

[a]College of Chemistry, State Key Laboratory of Elemento-Organic Chemistry, Nankai University, Tianjin 300071, China. E-mail: yuliu@nankai.edu.cn
[b]Collaborative Innovation Center of Chemical Science and Engineering, Tianjin 300072, P. R. China
[c]Key Laboratory of Molecular Microbiology and Technology, College of Life Sciences, Nankai University, Tianjin 300071, China

† Electronic supplementary information (ESI) available. See DOI: 10.1039/c9sc00026g

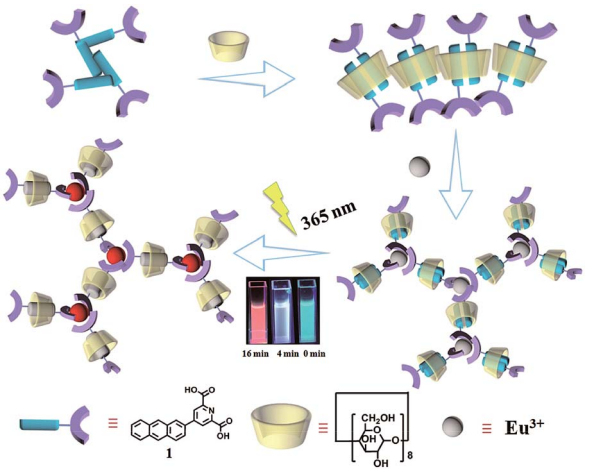

Fig. 1 Schematic illustration of the γ-cyclodextrin/anthracene/Eu^{3+} supramolecular assembly and tunable lanthanide luminescence driven by reversible photo-cyclodimerization.

Fig. 1. The complexation of γ-CD with **1** in a 1 : 2 molar ratio led to the formation of a pseudo[3]rotaxane in aqueous solution. Furthermore, Eu(III) could coordinate with the carboxylic groups of pseudo[3]rotaxanes resulting in the formation of a supramolecular network assembly. Significantly, multicolor fluorescence emission varying from cyan → white → red could be achieved by irradiating the pseudorotaxane network for 0–16 minutes, and these white light-containing multicolor emissions consequently enabled the potential application of the pseudorotaxane network as a tunable photochromic fluorescent ink and cell label. This supramolecular approach to obtain multicolor and white light emission by controlling the photoirradiation time would provide a new strategy for smart optical materials.

Experimental

Materials and methods

All chemicals were commercially available unless noted otherwise. Compound **4** was prepared according to the literature procedure.[16] Compounds **2**, **5** and **6** were purchased from Heowns. NMR spectroscopy was performed on a Bruker AV400 spectrometer. Fluorescence spectroscopy was performed in a conventional quartz cell (light path 10 mm) on a Varian Cary Eclipse equipped with a Varian Cary single-cell Peltier accessory to control temperature at 25 °C. UV/vis spectra and the optical transmittance were recorded at 25 °C in a quartz cell (light path 10 mm) on a Shimadzu UV-3600 spectrophotometer equipped with a PTC-348WI temperature controller. High-resolution Transmission electron microscopy (TEM) images were acquired using a Tecnai 20 high-resolution transmission electron microscope operating at an accelerating voltage of 200 keV. The sample for high-resolution TEM measurements was prepared by dropping the solution onto a copper grid. The grid was then air-dried. Scanning electron microscopy (SEM) images were obtained using a Hitachi S-3500N scanning electron microscope. Dynamic Light Scattering (DLS) spectroscopy was performed on a laser light scattering spectrometer (BI-200SM) equipped with a digital correlator (TurboCorr) at 636 nm at a scattering angle of 90°. The hydrodynamic diameter (Dh) was determined by DLS experiments at 25 °C. Electrospray ionization mass spectra (ESI-MS) were recorded using an Agilent 6520 Q-TOF-MS. Quantum yields were measured using an Edinburgh Instruments FS5 near-infrared spectrometer, with a 450 W xenon lamp as the excitation source. The 0.1 mM $Eu^{3+}\subset$γ-CD·$\mathbf{1}_2$ (pH = 9) solution was used to measure the quantum yield after irradiation for 0 min with an excitation wavelength of 365 nm, and the collection range was from 345 nm to 800 nm. The quantum yield of the $Eu^{3+}\subset$γ-CD·$\mathbf{1}_2$ solution after irradiation for 4 min and 16 min was respectively measured with an excitation wavelength of 290 nm, and the collection range was from 260 nm to 800 nm. Human lung adenocarcinoma cells (A549 cells, purchased from the Cell Resource Center, China Academy of Medical Science, Beijing, China) were cultured in F12 medium containing 10% fetal bovine serum (FBS). A549 cells were seeded in 96 well plates (5×10^4 cell mL^{-1}, 0.1 mL per well) for 24 h at 37 °C in 5% CO_2, and then incubated with $Eu^{3+}\subset$γ-CD·$\mathbf{1}_2$ ($[Eu^{3+}] = 2$ μM, [γ-CD] = 4 μM, $[\mathbf{1}_2] = 8$ μM) for another 24 h. The relative cellular viability was determined by the MTT assay. A549 cells were seeded in 6 well plates (5×10^4 cell mL^{-1}, 2 mL per well) for 24 h at 37 °C in 5% CO_2. The cells were incubated with the corresponding solution for 12 h. After removing the medium, the cells were washed with phosphate buffer solution three times and fixed with 4% paraformaldehyde for 15 min. Finally, the cells were subjected to observation under a confocal laser scanning microscope.

Synthesis of 3

A three neck flask was charged with **4** (181.2 mg, 0.6 mmol), **5** (111.0 mg, 0.5 mmol), K_2CO_3 (400.5 mg, 2.89 mmol), toluene (50 mL) and H_2O (12.5 mL), and the resulting solution was degassed *via* three freeze–pump–thaw cycles. $Pd(PPh_3)_4$ (107.2 mg, 0.0926 mmol) was then added under an argon atmosphere. The mixture was refluxed for about 1 h (monitored by TLC) resulting in a turbid solution. After the solvent was removed under vacuum, CH_2Cl_2 (50 mL) was added and washed with H_2O. The organic layer was dried with anhydrous Na_2SO_4 and filtered. After removal of CH_2Cl_2 under vacuum, the residue was purified by column chromatography on SiO_2 with CH_2Cl_2 as eluent to give a light yellow solid (110.2 mg, 61%). ^{1}H NMR (400 MHz, $CDCl_3$) δ 8.70 (s, 2H), 8.57 (s, 1H), 8.47 (d, J = 15.7 Hz, 2H), 8.17 (d, J = 8.8 Hz, 1H), 8.05 (s, 2H), 7.83 (d, J = 8.7 Hz, 1H), 7.54 (s, 2H), 4.56 (dd, J = 14.0, 6.9 Hz, 4H), 1.51 (t, J = 7.0 Hz, 6H). ^{13}C NMR (101 MHz, $CDCl_3$) δ 163.9, 149.8, 148.2, 131.8, 131.5, 131.2, 130.3, 130.1, 128.7, 127.3, 127.2, 126.6, 125.3, 125.2, 125.0, 124.5, 122.4, 98.9, 61.5, 13.2. HR-MS (ESI): *m*/*z* calcd for $C_{25}H_{21}NO_4$: 400.1549 $[M + H]^+$, found: 400.1547 (Fig. S1–S3†).

Synthesis of 1

Sodium hydroxide (30.3 mg, 0.75 mmol) was dissolved in water (10 mL) and a 10 mL THF solution of 3 (50.4 mg, 0.125 mmol) was added. The resulting suspension was stirred at 100 °C overnight and cooled to room temperature. After removal of THF under vacuum, the pH was adjusted to 1 using 37%

aqueous hydrogen chloride solution. The resulting precipitate was filtered, washed with water (3 × 30 mL) and dried under vacuum. The product was obtained as a yellow solid (37.4 mg, 74%). ^{1}H NMR (400 MHz, DMSO) δ 8.81 (s, 2H), 8.68 (s, 3H), 8.29 (d, J = 8.9 Hz, 1H), 8.14 (d, J = 6.5 Hz, 2H), 8.05 (d, J = 9.6 Hz, 1H), 7.64–7.51 (m, 2H). ^{13}C NMR (101 MHz, DMSO) δ 166.0, 150.2, 149.8, 145.9, 132.9, 132.5, 132.1, 131.5, 131.4, 130.0, 128.7, 128.6, 128.2, 128.0, 126.8, 126.5, 124.9, 124.2. HR-MS (ESI): m/z calcd for $C_{21}H_{13}NO_4$: 344.0924 $[M + H]^+$, found: 344.0918 (Fig. S4–S6†).

Determination of the association constant (K)

In the UV-vis titration experiments, the association constant (K_a) for a stoichiometric 1 : 2 complex (γ-CD·$\mathbf{1}_2$) of γ-CD with **1** was calculated by using the non-linear least-squares fit of the titration data according to the following formula with the Origin program.[17]

$$\Delta A_{obs} = \frac{\varepsilon_{\Delta HG}[G]_0 K_1[H] + 2\varepsilon_{\Delta HG_2}[G]_0 K_1 K_2[H]^2}{1 + K_1[H] + K_1 K_2[H]^2}$$

where ΔA_{obs} is the UV-vis absorption change of **1** upon addition of γ-CD. K_1 and K_2 are the first-order bonding constant and the second-order bonding constant, respectively. $\varepsilon_{\Delta HG}$ is the molar absorption coefficient change between the γ-CD·**1** inclusion complex and **1**. $\varepsilon_{\Delta HG^2}$ is the molar absorption coefficient change between the γ-CD·$\mathbf{1}_2$ inclusion complex and **1**. $[G]_0$ is the initial concentration of guest molecules.

Preparation of the Eu complex

Europium(III) nitrate hexahydrate ($Eu(NO_3)_3 \cdot 6H_2O$) was purchased from Energy Chemical. A certain amount of $Eu(NO_3)_3$ was dissolved in deionized water, and then added to the aqueous solution of **1** or γ-CD·$\mathbf{1}_2$ to prepare the Eu complex *in situ*. Preparation of $Eu^{3+}\subset\gamma$-CD·$\mathbf{1}_2$, *i.e.* the Eu complex of γ-CD·$\mathbf{1}_2$, as an example is as follows: a solution of $Eu(NO_3)_3$ (2 mM) was prepared in deionized water, and then 45 μL of the $Eu(NO_3)_3$ solution was added to the aqueous solution of γ-CD·$\mathbf{1}_2$ (0.1 mM, 3 mL) to obtain the $Eu^{3+}\subset\gamma$-CD·$\mathbf{1}_2$ solution (0.1 mM).

Results and discussion

1 was prepared in 74% yield *via* a Suzuki reaction of diethyl 4-bromopyridine-2,6-dicarboxylate with 2-anthraceneboronic acid under alkaline conditions, followed by a subsequent hydrolysis reaction (Scheme 1). It was reported that the γ-CD cavity could accommodate two 2-anthryl groups, and the 1 : 2 inclusion complex had four possible configurations including *syn* or *anti* head-to-tail (HT) and head-to-head (HH) isomers in aqueous solution.[18] Herein, a similar phenomenon was observed in aqueous solution. Fig S7a† shows the UV-vis absorption and fluorescence emission of **1**. The UV-vis spectra (Fig. 2a, S7b†) showed that, with the stepwise addition of γ-CD, the ^1B_b band of **1** at 260–280 nm gradually decreased, indicating the conformational change from the J-aggregate of self-assembled **1** to the H-aggregate of diploid **1** due to the inclusion of the γ-CD cavity.[18] In addition, the ^1L_a band of **1** at

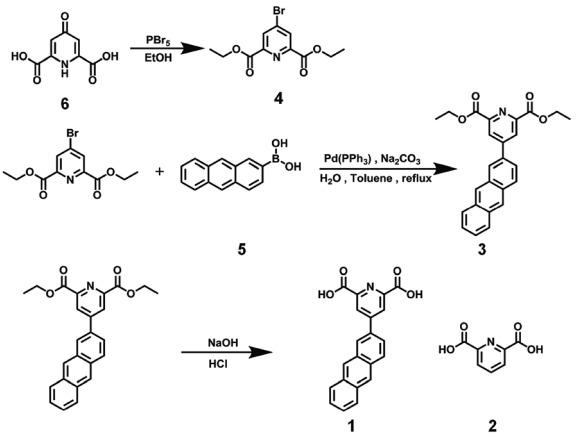

Scheme 1 Synthetic scheme of **1** and the structure of **2**.

410 nm showed a little bathochromic shift, and its intensity decreased. Moreover, two apparent isosbestic points at 319 nm and 400 nm were also observed. These phenomena jointly indicated the conversion of free **1** to the γ-CD·$\mathbf{1}_2$ inclusion complex.[19] Accordingly, the association constants (K_a) between **1** and γ-CD were calculated to be $K_{a1} = 4.38 \times 10^2$ M^{-1} and $K_{a2} = 5.58 \times 10^4$ M^{-1} at 25 °C by analyzing the sequential changes in UV-vis spectra (ΔA) of **1** at varying concentrations of γ-CD using a nonlinear least-squares curve-fitting method according to literature reports (Fig. 2a and S7c†).[17] The Job's plot gave an inflection point at a molar ratio of 0.667, corresponding to a 1 : 2 host–guest inclusion stoichiometry (Fig. S8†), which was consistent with the previously reported result.[19] To further prove the inclusion, ^{1}H NMR spectra (Fig. S9a, b†) showed that the anthracene protons shifted upfield 0.375–0.4 ppm upon complexation with γ-CD. In the circular dichroism spectra (Fig. S10†), the γ-CD·$\mathbf{1}_2$ inclusion complex (green line) showed

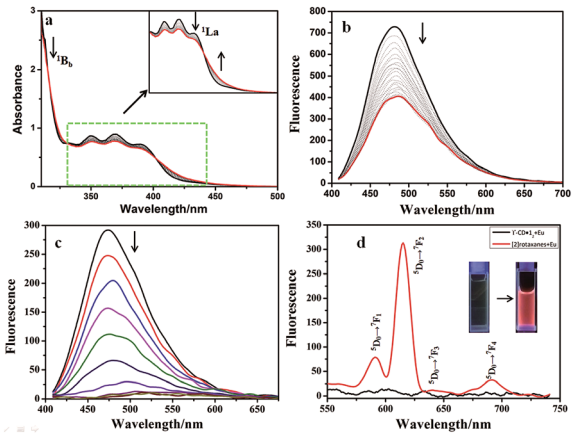

Fig. 2 (a) Absorption spectra and (b) emission spectra of **1** (0.2 mM) with (red) and without (black) γ-CD (0–0.3 mM) at pH 9.0 in water (25 °C). (c) Emission spectra of γ-CD·$\mathbf{1}_2$ (0.2 mM) upon addition of Eu^{3+} (from 0 to 3 eq.) at pH 9.0 in water (25 °C, λ_{ex} = 365 nm) (d) emission spectra of the $Eu^{3+}\subset\gamma$-CD·$\mathbf{1}_2$ system (black) and $Eu^{3+}\subset$[2]rotaxanes (red) at 25 °C. Inset: photo image of fluorescence in pH 9.0 aqueous solution under UV light (λ_{ex} = 254 nm, 254 nm used as an excitation source).

a positive Cotton effect peak at 350–400 nm and a negative Cotton effect peak at 400–450 nm, indicating the formation of a pseudo[3]rotaxane.[19c] In the fluorescence spectra (Fig. 2b), the fluorescence intensity of **1** appreciably decreased with the gradual addition of γ-CD, due to the π–π stacking of **1** in the hydrophobic γ-CD cavity. Considering the structure of **1** that has a bulky negatively charged substituent at the 2-position, we deduced that the two units of **1** tended to adopt a *syn* or *anti* head-to-tail (HT) conformation upon inclusion by γ-CD.

It was well reported that pyridine-2,6-dicarboxylic acid (DPA) could strongly coordinate lanthanide ions with a ratio of 3 : 1.[20] Similarly, the fluorescence spectra experiments showed a 1 : 3 coordination stoichiometry between Eu^{3+} and **1**, which was consistent with our previous observation (Fig. S11†).[13c] Possessing two terminal DPA units, the γ-CD·$\mathbf{1}_2$ complex also showed similar coordination behaviors with lanthanide ions (Fig. 2c). With the gradual addition of Eu^{3+} to the γ-CD·$\mathbf{1}_2$ complex, no characteristic fluorescence of Eu^{3+} could be observed, but the fluorescence at 480 nm, assigned to the intrinsic blue fluorescence of the ligand, was gradually quenched (Fig. 2c and d black line), similar to the previous report.[13c] A possible reason may be that the large aromatic conjugate system in the antenna molecule led to a mismatch between the lowest triplet state of the ligand and the first excited state of the lanthanide. It is well documented that anthracenes are photoresponsive and apt to undergo photodimerization under UV irradiation.[21] However, after irradiating the aqueous solution of $Eu^{3+}\subset$γ-CD·$\mathbf{1}_2$ under N_2 for 16 min at 365 nm with an intensity of 50 W, the resultant solution presented four characteristic emissions (Fig. 2d, red line) of Eu^{3+} at 590 nm ($^5D_0 \rightarrow {}^7F_1$), 615 nm ($^5D_0 \rightarrow {}^7F_2$), 645 nm ($^5D_0 \rightarrow {}^7F_3$) and 680 nm ($^5D_0 \rightarrow {}^7F_4$),[13] which were quite similar to those of $Eu^{3+}\subset\mathbf{2}_3$ (Fig. S12†). This means that an energy transfer (ET) process occurred from pyridine-2,6-dicarboxylic acid (DPA) to Eu^{3+}.[13c] In the ^{1}H NMR spectra, the proton signals at 7.0–7.6 ppm assigned to the anthracene group in **1** displayed an upfield shift (Fig. S9†), indicating that the two accommodated groups may undergo dimerization after UV light irradiation.[19c] Moreover, the ROESY spectrum (Fig. S13†) also showed clear NOE (Nuclear Overhauser Effect) correlations between the dimeric anthracene groups and the inner protons of γ-CD. In addition, the circular dichroism spectrum (Fig. S10†) of γ-CD·$\mathbf{1}_2$ after UV irradiation was obviously different from that before UV irradiation. The ESI-MS spectrum of $Eu^{3+}\subset$γ-CD·$\mathbf{1}_2$ after irradiation at 365 nm in water showed a clear signal at *m*/*z* 1981.1 assigned to the [2]rotaxane, while the ESI-MS spectrum of a highly concentrated THF solution of **1** after irradiation at 365 nm showed a signal at *m*/*z* 689.1 assigned to the dimer of **1** (Fig. S14, S15†). No ESI-MS signal of the photooxidized product was observed for the case of either **1** or γ-CD·$\mathbf{1}_2$. These phenomena jointly demonstrated that the two discrete units of **1** in the γ-CD cavity converted into a dimer, *i.e.* the γ-CD·$\mathbf{1}_2$ complex converted to a [2]rotaxane, after UV light irradiation, and the photodimerized product was the principal product. Therefore, a possible emission mechanism could be deduced as follows: the photo-dimerization of the two accommodated anthracene groups in the γ-CD cavity destroyed the large conjugated structure of γ-CD·$\mathbf{1}_2$, allowing the match of the lowest triplet state of the ligand to the first excited state of the lanthanide ion. As a result, the characteristic fluorescence of Eu^{3+} was presented.[13c]

Significantly, $Eu^{3+}\subset$γ-CD·$\mathbf{1}_2$ showed different emission colors with the changes of light irradiation times. Without light irradiation, $Eu^{3+}\subset$γ-CD·$\mathbf{1}_2$ only emitted the intrinsic blue fluorescence of the ligand (Fig. 3A) at 490 nm. After irradiating the solution of $Eu^{3+}\subset$γ-CD·$\mathbf{1}_2$ under N_2 at 365 nm for 16 min, the fluorescence emission of Eu^{3+} was gradually enhanced, and the emission color changed in the order of cyan (0 min) → pale yellow (2 min) → white (4 min) → orange (8 min) → red (16 min). Moreover, an obvious white-light point with the CIE coordinate (0.32 and 0.36) was observed in the CIE 1931 chromaticity diagram (Fig. 3B). A possible reason may be that, with continuous irradiation by UV light, $Eu^{3+}\subset$γ-CD·$\mathbf{1}_2$, which emitted cyan fluorescence, gradually converted to $Eu^{3+}\subset$[2]rotaxane that emitted red fluorescence. Therefore, at different time points, the $Eu^{3+}\subset$γ-CD·$\mathbf{1}_2$ system existed as the mixtures of blue-light species $Eu^{3+}\subset$γ-CD·$\mathbf{1}_2$ and red-light species $Eu^{3+}\subset$[2]rotaxane with different ratios, leading to multi-color emission including white light. In addition, fluorescence lifetime experiments showed that the decay curve in pH 9.0 water followed a double exponential decay with fluorescence lifetimes at $\tau_1 = 1.10$ ns and $\tau_2 = 5.97$ ns in the initial state, and no fluorescence lifetimes of lanthanide ions were observed. But the $Eu^{3+}\subset$γ-CD·$\mathbf{1}_2$ showed the fluorescence lifetimes of lanthanide ions at $\tau_1 = 251.88$ μs and $\tau_2 = 993.46$ μs after photoirradiation for 16 min (Fig. S16†). The quantum yields were 3.12% in the initial state, 2.67% at 4 min and 15.74% at 16 min. In the emission spectra of $Eu^{3+}\subset$γ-CD·$\mathbf{1}_2$ without photoirradiation, *i.e.* the case where the sample is made and no irradiation is performed, no appreciable emission color changes were observed (Fig. S17a†), indicating that the different emission colors are due to the irradiation induced rotaxane formation

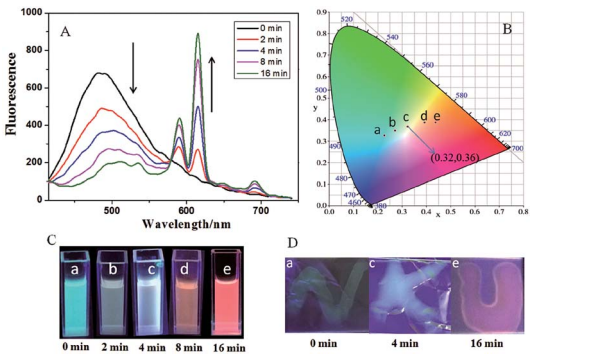

Fig. 3 (A) Emission spectra ($\lambda_{ex} = 290$ nm) of $Eu^{3+}\subset$γ-CD·$\mathbf{1}_2$ ([$\mathbf{1}_2$] = 0.1 mM and [Eu^{3+}] = 0.03 mM) in the initial state (a) and after photoirradiation for (b) 2 min, (c) 4 min, (d) 8 min, and (e) 16 min in pH = 9.0 aqueous solution at 25 °C; (B) CIE 1931 chromaticity diagram. The black dots signify the luminescent color coordinates for the corresponding states (a) (0.22, 0.32), (b) (0.27, 0.34), (c) (0.32, 0.36), (d) (0.39, 0.38), and (e) (0.43, 0.38). (C) The images of the corresponding states under UV irradiation ($\lambda_{ex} = 365$ nm), and (D) the features of fluorescent inks based on the $Eu^{3+}\subset$γ-CD·$\mathbf{1}_2$-doped PVA (the molar ratio is 1 : 500) film under UV irradiation ($\lambda_{ex} = 365$ nm).

rather than a simply slow coordination event. In the irradiation study of the $Eu^{3+}\subset\mathbf{1}_3$ complex (*i.e.* no CD present), very slight color changes were observed after irradiating the $Eu^{3+}\subset\mathbf{1}_3$ complex only, indicating that CD is required for the different emission colors because CD can not only increase the solubility of the guest, but also accelerate the dimerization (Fig. S17b†). Meanwhile, the changes of absorption spectra and the excitation spectra of $Eu^{3+}\subset\gamma\text{-CD}\cdot\mathbf{1}_2$ with photoirradiation are shown in Fig. S17c, d.† Furthermore, the morphology of $Eu^{3+}\subset$[2]rotaxane was investigated by scanning electron microscopy (SEM) and transmission electron microscopy (TEM) (Fig. S18, S19†). In SEM and TEM images, free **1** existed as a number of needle-like nanofibers, and $\gamma\text{-CD}\cdot\mathbf{1}_2$ showed the morphology as irregular blocks. However, the morphology of $Eu^{3+}\subset\gamma\text{-CD}\cdot\mathbf{1}_2$ before and after UV light irradiation both existed as thin films. In addition, the zeta potentials of free **1**, $\gamma\text{-CD}\cdot\mathbf{1}_2$, $Eu^{3+}\subset\gamma\text{-CD}\cdot\mathbf{1}_2$ were measured to be −29.44 mV, −10.63 mV and −4.45 mV (Fig. S20†), respectively, indicating that the coordination of Eu^{3+} decreased the surface electronegativity of **1** or $\gamma\text{-CD}\cdot\mathbf{1}_2$.

Benefitting from the photo-controlled multicolor emission properties, $Eu^{3+}\subset\gamma\text{-CD}\cdot\mathbf{1}_2$ could be used as a tunable photochromic fluorescent ink. In a typical test, some characters were written with the solution of $Eu^{3+}\subset\gamma\text{-CD}\cdot\mathbf{1}_2$-doped PVA as ink on an ordinary glass piece, and these characters emitted blue fluorescence under a UV lamp after being dried in air (Fig. 3). When irradiated with UV light (365 nm) from 0 min to 4 min, the characters emitted white fluorescence, which further turned red after irradiation for 16 min. Interestingly, these multi-color characters could remain stable for at least 72 h without any appreciable fading. Therefore, the tunable photochromic multicolor emission properties will enable the application of the $Eu^{3+}\subset\gamma\text{-CD}\cdot\mathbf{1}_2$ assembly as a novel anti-counterfeiting material in which information and the state could be effectively written and read out by simply alternating the UV irradiation time.

In addition to fluorescent ink, the $Eu^{3+}\subset\gamma\text{-CD}\cdot\mathbf{1}_2$ assembly could also be used as a photo-tunable multicolor fluorescent label for living cells. Firstly, we study its luminescence behavior under physiological conditions in PBS buffer (pH = 7.2). The $Eu^{3+}\subset\gamma\text{-CD}\cdot\mathbf{1}_2$ assembly exhibits red luminescence (at 254 nm) and white luminescence (at 365 nm) after light irradiation (Fig. 4a, S21a†). Accordingly, UV-vis absorption and fluorescence measurements were performed to monitor the photodimerization process of anthracene. Irradiation of the $Eu^{3+}\subset\gamma\text{-CD}\cdot\mathbf{1}_2$ under N_2 with 365 nm light using a portable UV lamp (6 W) decreased the intensity of absorption bands at 373 nm (assigned to the π–π* transition bands of anthracene units) and the fluorescence intensity at 494 nm gradually declined, indicating that the photodimerization disrupted the conjugation of anthracene units (Fig. 4a, c).[21,22] The fluorescence lifetime decay curve of $Eu^{3+}\subset\gamma\text{-CD}\cdot\mathbf{1}_2$ in PBS buffer (pH = 7.2) also showed the fairly high fluorescence lifetimes of the lanthanide ion up to τ_1 = 543.50 μs and τ_2 = 1204.91 μs after photoirradiation (Fig. S22†). Moreover, the reversibility of such luminescence properties is highly desired for wide applications and thus we examined its reversibility. When $Eu^{3+}\subset$[2]rotaxane was irradiated at 254 nm for 120 s, a reconversion to the parent species $Eu^{3+}\subset\gamma\text{-CD}\cdot\mathbf{1}_2$ occurred, as confirmed by UV-vis absorption and fluorescence

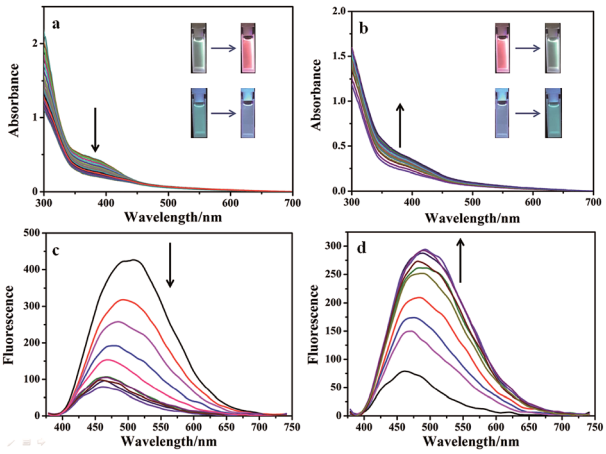

Fig. 4 Absorption spectral changes of $Eu^{3+}\subset\gamma\text{-CD}\cdot\mathbf{1}_2$ (0.1 mM) upon irradiation (a) at 365 nm and (b) at 254 nm in PBS at 25 °C (pH = 7.2, inset: the upper and lower images for the fluorescence changes at an excitation wavelength of 254 nm and 365 nm, respectively). Fluorescence spectral changes of $Eu^{3+}\subset\gamma\text{-CD}\cdot\mathbf{1}_2$ upon photoirradiation (c) at 365 nm and (d) at 254 nm in PBS at 25 °C (λ_{ex} = 365 nm).

measurements (Fig. 4b, d). Significantly, cycle tests showed that the external-stimuli-responsive transformation is repetitive (Fig. S21b, S23†). The solution of free **1** and $Eu^{3+}\subset\mathbf{1}_3$ quickly precipitated as shown in Fig. S21c.† Simultaneously, the fluorescence of $Eu^{3+}\subset\mathbf{1}_3$ is very weak, and red fluorescence is not observed after irradiation at 365 nm for 3 h or even longer (Fig. S21a†). We then treated human lung adenocarcinoma cells (A549 cells) with the $Eu^{3+}\subset\gamma\text{-CD}\cdot\mathbf{1}_2$ assembly for 24 h. The cytotoxicity of the assembly was evaluated by using a standard MTT assay. As shown in Fig. S24,† over 90% cell viability is observed after incubation of A549 cells with the assembly at concentrations ranging from 1 to 16 μM for 24 h, thus confirming the low cytotoxicity of the assembly. Confocal laser scanning microscopy revealed that the cells initially emitted blue fluorescence in the cytoplasm under UV irradiation (365 nm) (Fig. 5a), and then gradually emitted white fluorescence after 1 min of irradiation, which remained stable for further irradiation

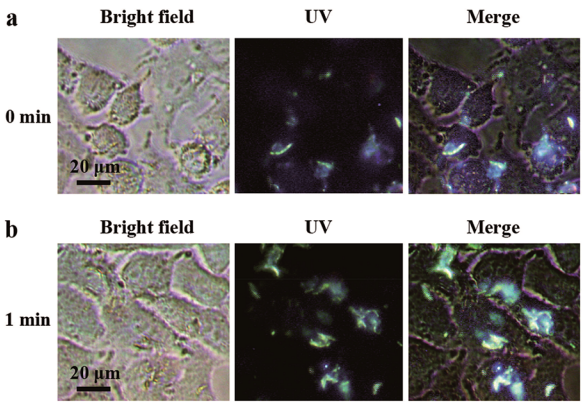

Fig. 5 Confocal fluorescence images of A549 cells incubated with $Eu^{3+}\subset\gamma\text{-CD}\cdot\mathbf{1}_2$ ([Eu^{3+}] = 2 μM, [γ-CD] = 4 μM, and [$\mathbf{1}_2$] = 8 μM) after irradiation for (a) 0 min and (b) 1 min under UV light at 25 °C.

(Fig. 5b). Thus, this assembly could be used to tag cells with white fluorescence. As we know, most of the fluorescent dyes only exhibit blue, green, red or yellow fluorescence during cell imaging.[15,23] It is necessary to develop novel staining systems with other fluorescence emission properties when more than four fluorescence signals are needed. The $Eu^{3+}\subset\gamma$-CD·$\mathbf{1}_2$ assembly with white light emission provides the fifth kind of fluorescence signal, and hence would have wide application in multi-color imaging for biological studies.

Conclusions

In conclusion, we have successfully constructed a photo-tunable supramolecular assembly from γ-CD, anthracene-modified DPA and lanthanide metal *via* the time-dependent photo-crosslinking reaction. The resultant supramolecular assembly possessed dual emission properties, *i.e.* a red-light emission of Eu(III) and a blue-light emission of anthyl-modified DPA. Through controllably adjusting the light irradiation time, the supramolecular assembly could emit fluorescence with various colors (especially white light) in several environments such as aqueous solution, solid films and especially living cells, which enabled the potential application of this photo-tunable multi-color assembly as a tunable photochromic fluorescent ink and cell label. We believe that this study could provide a new strategy for information processing and biological imaging.

Conflicts of interest

There are no conflicts to declare.

Acknowledgements

We thank NNSFC (21672113, 21432004, 21772099, 21861132001 and 91527301) for financial support.

Notes and references

1 (*a*) L. Fang, M. A. Olson, D. Benitez, E. Tkatchouk, W. A. Goddard and J. F. Stoddart, *Chem. Soc. Rev.*, 2010, **39**, 17–29; (*b*) H. X. Wang, Z. Meng, J. F. Xiang, Y. X. Xia, Y. H. Sun, S. Z. Hu, H. Chen, J. N. Yao and C. F. Chen, *Chem. Sci.*, 2016, **7**, 469–474; (*c*) Z. J. Zhang, H. Y. Zhang, H. Wang and Y. Liu, *Angew. Chem., Int. Ed.*, 2011, **50**, 10834–10838.

2 (*a*) K. Iwaso, Y. Takashima and A. Harada, *Nat. Chem.*, 2016, **8**, 625–632; (*b*) M. R. Panman, C. N. van Dijk, A. Huerta-Viga, H. J. Sanders, B. H. Bakker, D. A. Leigh, A. M. Brouwer, W. J. Buma and S. Woutersen, *Nat. Commun.*, 2017, **8**, 1.

3 (*a*) A. Ulfkjaer, F. W. Nielsen, H. Al-Kerdi, T. Ruβ, Z. K. Nielsen, J. Ulstrup, L. L. Sun, K. Moth-Poulsen, J. D. Zhang and M. Pittelkow, *Nanoscale*, 2018, **10**, 9133–9140; (*b*) M. W. Ambrogio, C. R. Thomas, Y. L. Zhao, J. I. Zink and J. F. Stoddart, *Acc. Chem. Res.*, 2011, **44**, 903–913.

4 (*a*) S. Erbas-Cakmak, S. D. P. Fielden, U. Karaca, D. A. Leigh, C. T. McTernan, D. J. Tetlow and M. R. Wilson, *Science*, 2017, **358**, 340–343; (*b*) S. Kassem, A. T. L. Lee, D. A. Leigh, V. Marcos, L. I. Palmer and S. Pisano, *Nature*, 2017, **549**, 374–378; (*c*) M. Mohankumar, M. Holler, E. Meichsner, J. F. Nierengarten, F. Niess, J. P. Sauvage, B. Delavaux-Nicot, E. Leoni, F. Monti, J. M. Malicka, M. Cocchi, E. Bandini and N. Armaroli, *J. Am. Chem. Soc.*, 2018, **140**, 2336–2347.

5 (*a*) X. Ma and H. Tian, *Chem. Soc. Rev.*, 2010, **39**, 70–80; (*b*) X. Hou, C. Ke, C. J. Bruns, P. R. McGonigal, R. B. Pettman and J. F. Stoddart, *Nat. Commun.*, 2015, **6**, 6884; (*c*) M. Inouye, K. Hayashi, Y. Yonenaga, T. Itou, K. Fujimoto, T. Uchida, M. Iwamura and K. Nozaki, *Angew. Chem., Int. Ed.*, 2014, **53**, 14392–14396; (*d*) L. D. Movsisyan, M. Franz, F. Hampel, A. L. Thompson, R. R. Tykwinski and H. L. Anderson, *J. Am. Chem. Soc.*, 2016, **138**, 1366–1376.

6 (*a*) G. M. Farinola and R. Ragni, *Chem. Soc. Rev.*, 2011, **40**, 3467–3482; (*b*) O. Kotova, S. Comby, C. Lincheneau and T. Gunnlaugsson, *Chem. Sci.*, 2017, **8**, 3419–3426; (*c*) S. Reineke, F. Lindner, G. Schwartz, N. Seidler, K. Walzer, B. Lussem and K. Leo, *Nature*, 2009, **459**, 234–238.

7 (*a*) B. W. D'Andrade and S. R. Forrest, *Adv. Mater.*, 2004, **16**, 1585–1595; (*b*) K. T. Kamtekar, A. P. Monkman and M. R. Bryce, *Adv. Mater.*, 2010, **22**, 572–582; (*c*) L. L. Zhu, C. Y. Ang, X. Li, K. T. Nguyen, S. Y. Tan, H. Agren and Y. L. Zhao, *Adv. Mater.*, 2012, **24**, 4020–4024.

8 (*a*) M. M. Shang, C. X. Li and J. Lin, *Chem. Soc. Rev.*, 2014, **43**, 1372–1386; (*b*) N. Willis-Fox, M. Kraft, J. Arlt, U. Scherf and R. C. Evans, *Adv. Funct. Mater.*, 2016, **26**, 532–542; (*c*) X. Feng, C. X. Qi, H. T. Feng, Z. Zhao, H. H. Y. Sung, I. D. Williams, R. T. K. Kwok, J. W. Y. Lam, A. J. Qin and B. Z. Tang, *Chem. Sci.*, 2018, **9**, 5679–5687.

9 (*a*) R. Abbel, C. Grenier, M. J. Pouderoijen, J. W. Stouwdam, P. E. L. G. Leclere, R. P. Sijbesma, E. W. Meijer and A. P. H. J. Schenning, *J. Am. Chem. Soc.*, 2009, **131**, 833–843; (*b*) Z. Y. Zhang, B. Xu, J. H. Su, L. P. Shen, Y. S. Xie and H. Tian, *Angew. Chem., Int. Ed.*, 2011, **123**, 11858–11861; (*c*) Q. Zhao, Y. Chen, S. H. Li and Y. Liu, *Chem. Commun.*, 2018, **54**, 200–203.

10 Q. W. Zhang, D. F. Li, X. Li, P. B. White, J. Mecinovic, X. Ma, H. Agren, R. J. M. Nolte and H. Tian, *J. Am. Chem. Soc.*, 2016, **138**, 13541–13550.

11 X. L. Ni, S. Y. Chen, Y. P. Yang and Z. Tao, *J. Am. Chem. Soc.*, 2016, **138**, 6177–6183.

12 S. H. Li, X. F. Xu, Y. Zhou, Q. Zhao and Y. Liu, *Org. Lett.*, 2017, **19**, 6650–6653.

13 (*a*) H. B. Cheng, H. Y. Zhang and Y. Liu, *J. Am. Chem. Soc.*, 2013, **135**, 10190–10193; (*b*) M. Isaac, S. A. Denisov, A. Roux, D. Imbert, G. Jonusauskas, N. D. McClenaghan and O. Seneque, *Angew. Chem.*, 2015, **127**, 11615–11618; (*c*) Y. Zhou, H. Y. Zhang, Z. Y. Zhang and Y. Liu, *J. Am. Chem. Soc.*, 2017, **139**, 7168–7171; (*d*) B. McMahon and T. Gunnlaugsson, *J. Am. Chem. Soc.*, 2012, **134**, 10725–10728; (*e*) O. Kotova, R. Daly, C. M. G. dos Santos, M. Boese, P. E. Kruger, J. J. Boland and T. Gunnlaugsson, *Angew. Chem.*, 2012, **51**, 7208–7212.

14 H. Wu, Y. Chen and Y. Liu, *Adv. Mater.*, 2017, **29**, 1605271.

15 X.-M. Chen, Y. Chen, Q. L. Yu, B.-H. Gu and Y. Liu, *Angew. Chem., Int. Ed.*, 2018, **57**, 12519–12523.
16 K. E. Pryor, G. W. Shipps Jr, D. A. Skyler and J. Rebek Jr, *Tetrahedron*, 1998, **54**, 4107–4124.
17 (*a*) P. Thordarson, *Chem. Soc. Rev.*, 2011, **40**, 1305–1323; (*b*) H. Bakirci, X. Zhang and W. M. Nau, *J. Org. Chem.*, 2005, **70**, 39–46.
18 (*a*) A. Wakai, H. Fukasawa, C. Yang, T. Mori and Y. Inoue, *J. Am. Chem. Soc.*, 2012, **134**, 4990–4997; (*b*) Q. Wang, C. Yang, C. F. Ke, G. Fukuhara, T. Mori, Y. Liu and Y. Inoue, *Chem. Commun.*, 2011, **47**, 6849–6851; (*c*) C. Yang and Y. Inoue, *Chem. Soc. Rev.*, 2014, **43**, 4123–4143.
19 (*a*) A. Nakamura and Y. Inoue, *J. Am. Chem. Soc.*, 2003, **125**, 966–972; (*b*) X. Q. Wei, W. H. Wu, R. Matsushita, Z. Q. Yan, D. Y. Zhou, J. J. Chruma, M. Nishijima, G. Fukuhara, T. Mori, Y. Inoue and C. Yang, *J. Am. Chem. Soc.*, 2018, **140**, 3959–3974; (*c*) C. Yang, T. Mori, Y. Origane, Y. H. Ko, N. Selvapalam, K. Kim and Y. Inoue, *J. Am. Chem. Soc.*, 2008, **130**, 8574–8575.
20 (*a*) Z. Q. Li, G. N. Wang, Y. G. Wang and H. R. Li, *Angew. Chem., Int. Ed.*, 2018, **57**, 2194–2198; (*b*) Y. Liu, G. S. Chen, Y. Chen, N. Zhang, J. Chen and Y. L. Zhao, *Nano Lett.*, 2006, **6**, 2196–2200.
21 (*a*) Z. A. Huang, C. Chen, X. D. Yang, X. B. Fan, W. Zhou, C. H. Tung, L. Z. Wu and H. Cong, *J. Am. Chem. Soc.*, 2016, **138**, 11144–11147; (*b*) D. J. Murray, D. D. Patterson, P. Payamyar, R. Bhola, W. T. Song, M. Lackinger, A. D. Schluter and B. T. King, *J. Am. Chem. Soc.*, 2015, **137**, 3450–3453; (*c*) T. Yamamoto, S. Yagyu and Y. Tezuka, *J. Am. Chem. Soc.*, 2016, **138**, 3904–3911; (*d*) P. F. Wei, X. Z. Yan and F. H. Huang, *Chem. Commun.*, 2014, **50**, 14105–14108; (*e*) G. Collet, T. Lathion, C. Besnard, C. Piguet and S. Petoud, *J. Am. Chem. Soc.*, 2018, **140**, 10820–10828.
22 (*a*) H. Bouas-Laurent, A. Castellan, J.-P. Desvergnea and R. Lapouyade, *Chem. Soc. Rev.*, 2000, **29**, 43–55; (*b*) N. Huang, X. Ding, J. Kim, H. Ihee and D. Jiang, *Angew. Chem., Int. Ed.*, 2015, **54**, 8704–8707.
23 (*a*) K. Jiang, S. Sun, L. Zhang, Y. Lu, A. Wu, C. Cai and H. Lin, *Angew. Chem., Int. Ed.*, 2015, **54**, 5360–5363; (*b*) Q. L. Yu, Y.-M. Zhang, Y.-H. Liu, X. Xu and Y. Liu, *Sci. Adv.*, 2018, **4**, eaat2297; (*c*) G. C. Yu, Z. Yang, X. Fu, B. C. Yung, J. Yang, Z. W. Mao, L. Shao, B. Hua, Y. Liu, F. Zhang, Q. Fan, S. Wang, O. Jacobson, A. Jin, C. Y. Gao, X. Tang, F. H. Huang and X. Y. Chen, *Nat. Commun.*, 2018, **9**, 9.